

The Study of Microstructure and Electrochemical Properties of Melt-spun Mg-Ni-La alloys

Huang Lin-jun*, Wang Yan-xin, Tang Jian-guo, Liu Jing-quan, Wang Yao, Liu Ji-xian Huang Zhen

College of Chemistry, Chemical and Environmental Engineering, Laboratory of New Fiber Materials and Modern Textile, the Growing Base for State Key Laboratory, Qingdao University, Qingdao 266071, China

*E-mail: newboy66@126.com

Received: 30 September 2011 / Accepted: 7 November 2011 / Published: 1 December 2011

Amorphous and nanocrystalline Mg-based alloys ($(\text{Mg}_{70.6}\text{Ni}_{29.4})_{100-x}\text{La}_x$ ($x=2, 5, 8, 10, 15\text{mol}\%$) were prepared by rapid solidification. The microstructure of the as-quenched ribbons and the electrochemical properties of these alloys with different La content were characterized and measured. The experimental results showed that the degree of short-range order increased with increasing La atomic content. The highest discharge capacity reached more than 564.2 mAhg^{-1} for $(\text{Mg}_{70.6}\text{Ni}_{29.4})_{92}\text{La}_8$ samples. Its capacity conservation rate was 85% after 10 cycles. The discharge capacities reached more than 300 mAhg^{-1} for $(\text{Mg}_{70.6}\text{Ni}_{29.4})_{98}\text{La}_2$ and $(\text{Mg}_{70.6}\text{Ni}_{29.4})_{98}\text{La}_2$ samples. Their discharge-capacities were improved greatly compared with the Mg_2Ni crystalline alloys. It was confirmed that the increase of discharge capacities is not only a function of the sample composition but strongly influenced by the amorphous phase proportion in the alloys.

Keywords: Mg-Ni-La hydrogen-storage alloy; microstructure; Electrochemical properties; Amorphous alloy

1. INTRODUCTION

Mg-based hydrogen storage alloys have been regarded as one of the most promising candidates as anode materials of Ni-MH batteries, because of their high hydrogen storage capacity, light weight, abundant supply and low cost [1,2]. However, their poor dehydrogenation kinetics at room temperature and serious degradation of the discharge capacity during electrochemical cycles caused them to be far from practical applications. For example, Cui et al. [3] reported that the discharge capacity of the as-cast Mg_2Ni alloy was only 8 mAh g^{-1} , far below its theoretical value of 999 mAhg^{-1} . Usually, the discharge capacity degradation of Mg-based hydrogen storage alloys is interpreted as the result of the

corrosion of alloys in alkaline solutions and the pulverization of alloy particles during charge/discharge cycles[4,5].

In recent years, Amorphous and nanocrystalline structures have proved to be beneficial to the improvement of the electrochemical properties of Mg-based alloys [6–10]. Such nonequilibrium structures were usually obtained by ball milling [11–13] and rapid solidification [14–16]. In addition, some other techniques, such as the equal channel angular pressing (ECAP) technique [17], were also employed to produce such structures. The rare earth elements (La, Nd) were often introduced into the alloys to enhance the glass forming ability in melt-spinning technique [18]. Thus, the discharge capacities of the alloys were remarkably increased [19,20]. In a series of our previous papers the crystallization, microstructure and the hydrogen storage properties for various rapidly Mg-Ni-Nd amorphous alloys were studied [21–23]. This paper presents our microstructure and electrochemical properties study of Mg-Ni-La alloys with nanocrystalline/amorphous structure.

2. EXPERIMENTAL

(Mg_{70.6}Ni_{29.4})_{100-x}La_x (x=2, 5, 8, 10, 15mol%) alloy ingot was prepared by induction melting a mixture of pure La metal and Mg-Ni alloy in a vacuum furnace under the protection of argon gas. Based on the low melting point and the high vapor pressure of Mg, a special melting technique, that is positive pressure protection and repeated melting, has to be taken to prevent massive Mg evaporation and ensure composition homogeneity during master alloy ingot preparation. The amorphous ribbons were produced by a single roller melt-spun technique (copper quenching disc with a diameter of 250mm and surface velocity of about 39ms⁻¹) in a argon atmosphere of 400mbar. The ribbons were about 2mm wide and 20 μm thick.

In electrochemical measurement, the amorphous alloy ribbons were fixed in a special mold to form the negative electrode.

The positive electrode was made of Ni-oxyhydroxide/dihydroxide. The alkaline solution was 6mol/l KOH containing 20g/l LiOH. The specimens were charged at 100mA g⁻¹ for 12h and discharged at 50mA g⁻¹ using the BTW-2000 battery testing instrument (Arbin). The discharged cut-off potential was set to 0.8 V between the two electrodes. The resting time between the charge and discharge was 1 h.

The microstructural characterization of the ribbons before and after charge/discharge cycles was confirmed by high resolution transmission electron microscopy (HRTEM, JEOL-2010) and by X-ray (using Cu k_α radiation) and electron diffraction.

3. RESULTS AND DISCUSSION

Fig.1 and Fig.2 presents the X-ray diffraction patterns of the as-quenched (Mg_{70.6}Ni_{29.4})_{100-x}La_x (x=2, 5, 8, 10, 15mol%) alloys. It is seen that the as-quenched (Mg_{70.6}Ni_{29.4})₉₈La₂ alloy reveals a

nanocrystalline structure corresponding to Mg_2Ni and $MgNi_2$ phases. $(Mg_{70.6}Ni_{29.4})_{95}La_5$ alloy shows a nanocrystalline structure with some amorphous phases. By indexing, the nano-crystalline phase Mg_2Ni is detected.

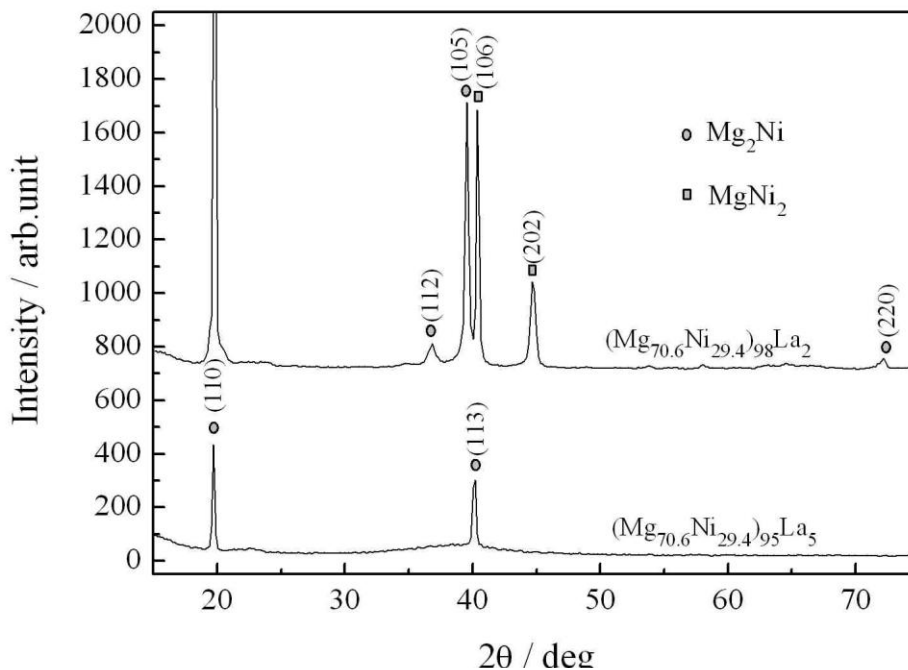


Figure 1. X-ray diffraction patterns of $(Mg_{70.6}Ni_{29.4})_{98}La_2$ and $(Mg_{70.6}Ni_{29.4})_{95}La_5$ alloys

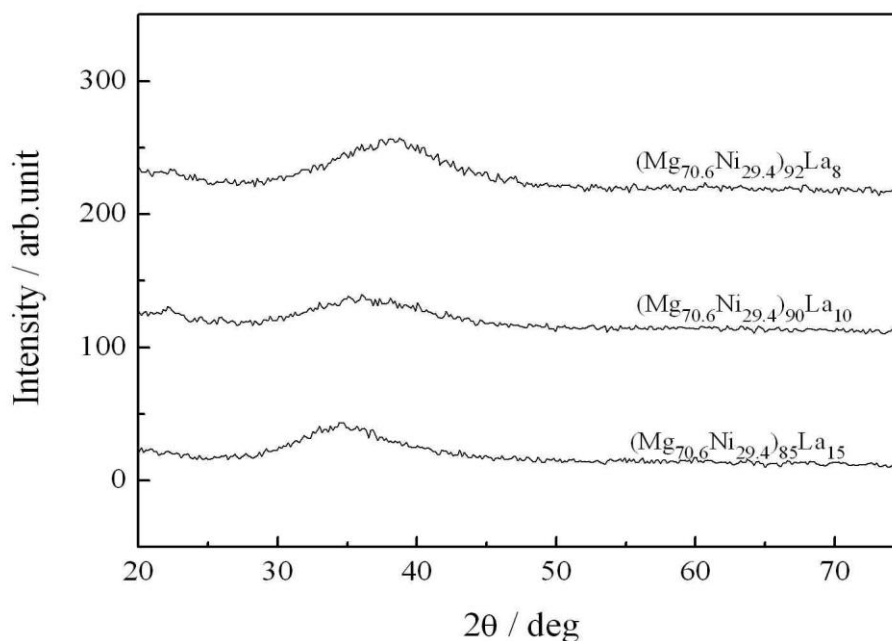


Figure 2. X-ray diffraction patterns of $(Mg_{70.6}Ni_{29.4})_{92}La_8$, $(Mg_{70.6}Ni_{29.4})_{90}La_{10}$ and $(Mg_{70.6}Ni_{29.4})_{85}La_{15}$ alloys

When the La content exceeds 5 mol%, the alloys $(Mg_{70.6}Ni_{29.4})_{92}La_8$, $(Mg_{70.6}Ni_{29.4})_{90}La_{10}$, and $(Mg_{70.6}Ni_{29.4})_{85}La_{15}$ all show only a broad and diffuse peak, namely the featureless appearance is typical of amorphous structure. It is also seen from Fig.2 that the typical amorphous peaks get low and even with the La content increasing, which implies more uniform of elements in the amorphous structure.

According to Scherrer formula, Table 1 gives the results of short-range order for amorphous alloys with different La content. It can be seen from Table 1, with the La content increases, the short-range order for different ribbons becomes small. That means the increasing of La content strengthen the degree of alloy amorphization .

Table 1. The short-range order of amorphous alloys with different La content

Alloys	Values of short-range order / nm
$(Mg_{70.6}Ni_{29.4})_{92}La_8$	1.086
$(Mg_{70.6}Ni_{29.4})_{90}La_{10}$	1.076
$(Mg_{70.6}Ni_{29.4})_{85}La_{15}$	1.047

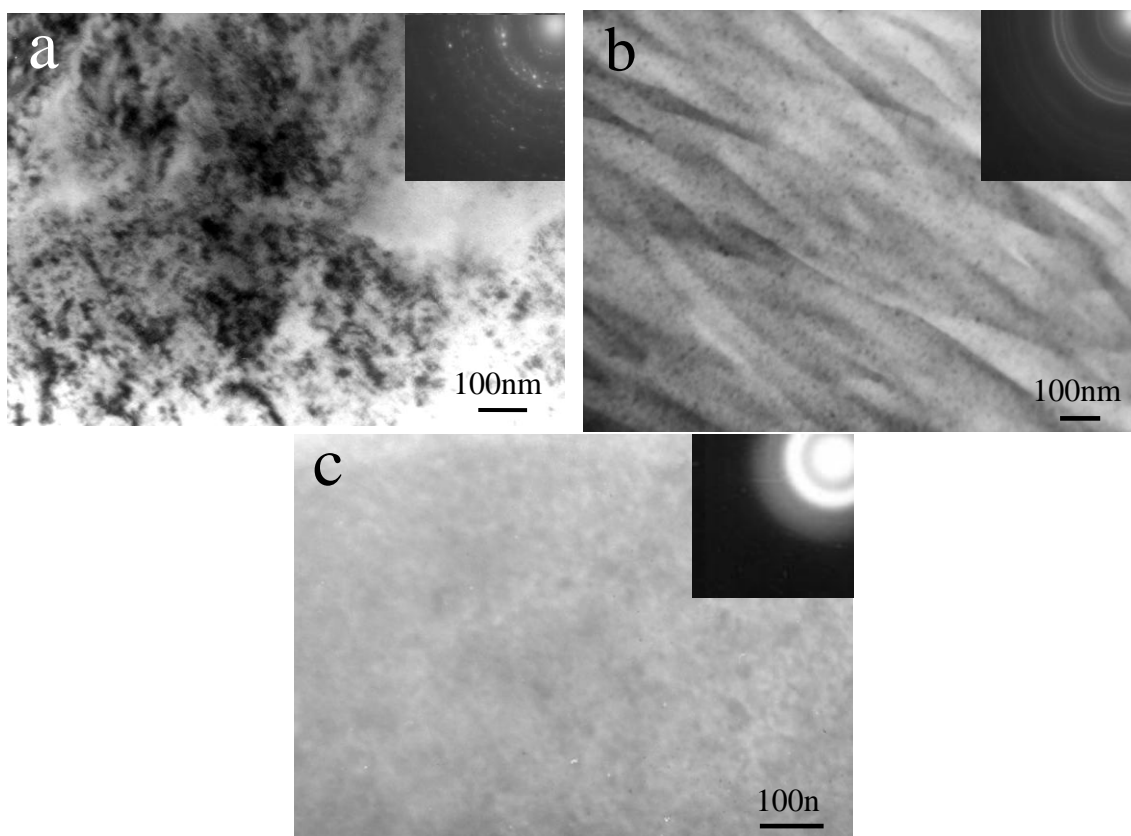


Figure 3. HRTEM image and electron diffraction pattern of as-quenched Mg-Ni-La alloys. (a) $(Mg_{70.6}Ni_{29.4})_{98}La_2$ (b) $(Mg_{70.6}Ni_{29.4})_{95}La_5$ (c) $(Mg_{70.6}Ni_{29.4})_{92}La_8$

Fig. 3 a shows the high-resolution transmission electron microscopy images of sample $(\text{Mg}_{70.6}\text{Ni}_{29.4})_{98}\text{La}_2$. It showed that a nano-crystalline structure with a few residual amorphous phases was obtained. Crystalline phase Mg_2Ni and MgNi_2 with average grain size in the range 30–50nm (Figs. 1 and Fig. 2 a).

The TEM image of as-quenched $(\text{Mg}_{70.6}\text{Ni}_{29.4})_{95}\text{La}_5$ alloy is shown in Fig.3 b. It was found that the orthorhombic Mg_2Ni structure with average grain size in the range 10–20nm was detected from the electron diffraction pattern and Fig. 1, and a typical wide diffraction ring of amorphous structure presented in the XRD pattern. It was presumed that the nanocrystalline Mg_2Ni was embedded in the amorphous matrix. The Fig.3 C shows the TEM image and electron diffraction pattern of as-quenched $(\text{Mg}_{70.6}\text{Ni}_{29.4})_{92}\text{La}_8$ alloy, it was found that a uniform amorphous structure was obtained.

Fig. 4 shows the variation of the discharge capacity of the different samples versus the number of cycles. It can be observed that whatever the cycle number is, $(\text{Mg}_{70.6}\text{Ni}_{29.4})_{92}\text{La}_8$ has the highest capacity and $(\text{Mg}_{70.6}\text{Ni}_{29.4})_{98}\text{La}_2$ has the lowest one. For each composition, with increasing cycle numbers the discharge capacity reaches a maximum after three or four cycles, and then decreases for upper cycle numbers. The curves of the discharge capacity turn to smooth after 6 cycles. The largest discharge capacity of samples reached $347.8\text{mAh}\cdot\text{g}^{-1}$ for 2 mol% La, $461.9\text{mAh}\cdot\text{g}^{-1}$ for 5mol% La, $564.2\text{mAh}\cdot\text{g}^{-1}$ for 8mol% La, $480.3\text{mAh}\cdot\text{g}^{-1}$ for 10mol% La, and $456.3\text{mAh}\cdot\text{g}^{-1}$ for 15mol% La.

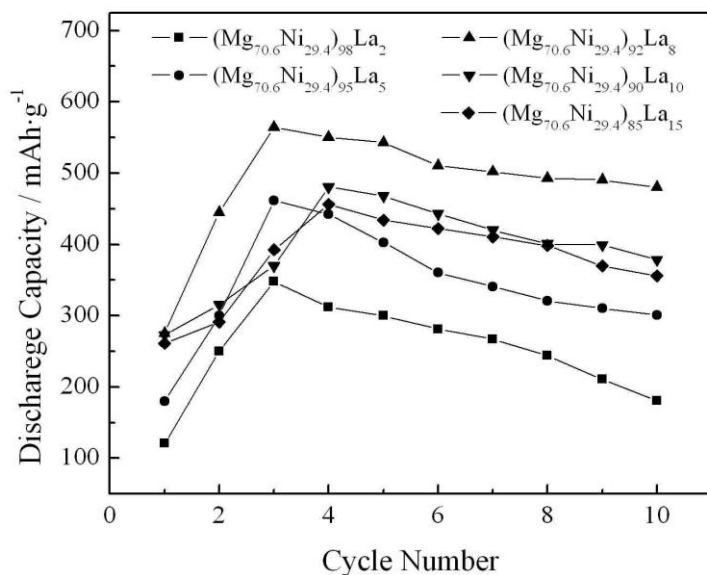


Figure 4. Variation of the discharge capacity vs. the cycle number for the different samples

Fig. 5 shows the XRD patterns of the charged $(\text{Mg}_{70.6}\text{Ni}_{29.4})_{92}\text{La}_8$ sample for three cycles. Because the sample contains 50 wt.% of nickel powder, three strong characteristic diffraction peaks of Ni are present. It is obvious that Mg_2NiH_4 phase forms during the charging process. The amorphous background concealed by the strong Ni peaks shows some amorphous phase remains. The crystallinity of $(\text{Mg}_{70.6}\text{Ni}_{29.4})_{92}\text{La}_8$ alloy calculated from Fig. 5 is about 74%, that is, the percentage of residual amorphous phase is 26%. The H atoms in the alloy are mainly stored in two regions, i.e. one part in the amorphous phase and the other part in the Mg_2NiH_4 phase. The crystallization behavior of the

(Mg_{70.6}Ni_{29.4})₉₂La₈ alloy after hydrogenation is different from the result reported by Spassov and Koster [24], which showed that the hydrogenation slightly decreased the thermal stability but strongly influenced the secondary crystallization of the as-quenched amorphous Mg₈₇Ni₁₂Y₁ alloy.

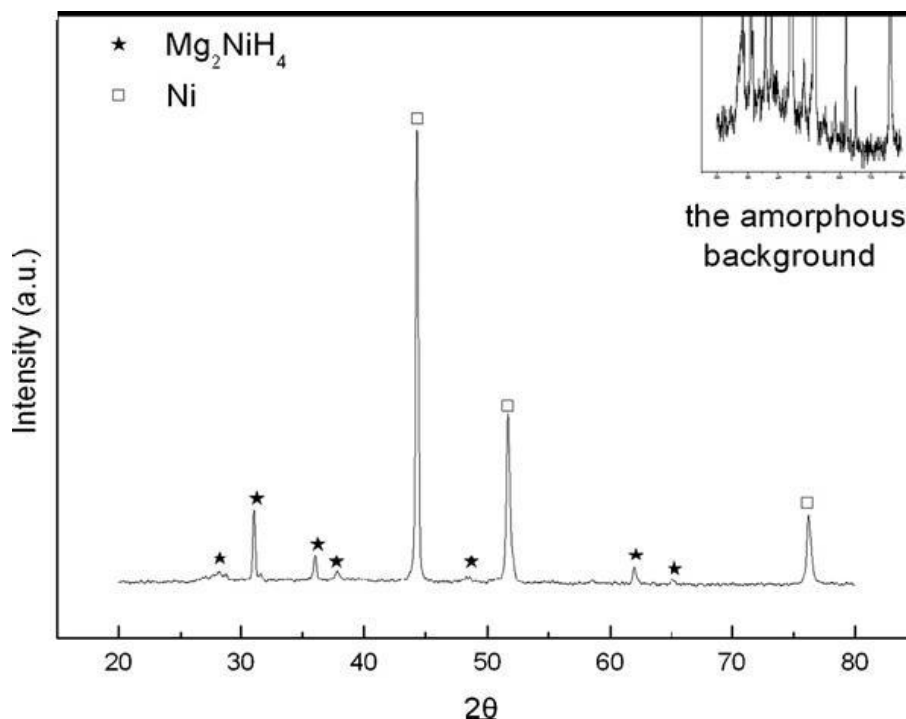


Figure 5. XRD patterns of amorphous (Mg_{70.6}Ni_{29.4})₉₂La₈ alloy charged at 3 cycle. clesdischarge capacity vs. the cycle number for the different samples.

Table 2 shows the values of the theoretical capacity, the maximum discharge capacity and theory utilization rate of Mg-Ni-La alloys calculated according to the formation hydride Mg₂NiH₄.

From above results, it is evident that the increase in discharge capacities is not only a function of the sample composition but also strongly influenced by the amorphous phase proportion in the alloyed material. As the content of La increases, the diffraction peak at about 40° shifts to lower angle (Fig. 1, 2). As we all know, the peak position of diffuse maxima is influenced by the average atomic distances in the amorphous matrix (short-range order).

In Fig. 2, the peak shift to lower positions is perhaps related to the larger atomic radius of the additional La and consequently, the higher the concentration the lower the position of the diffuse peak. That would enhance hydrogen diffusivity and solubility in amorphous and disordered structures, associated with the wide energy distribution of the available sites for hydrogen in the glassy structure as well as avoiding the long-range diffusion of hydrogen through an already formed hydride.

Table 2. The theory capacity, maximum discharge-capacity and theory utilization rate of Mg-Ni-La alloys

Alloys	Theory capacity /mAh·g ⁻¹	Maximum discharge-capacity /mAh·g ⁻¹	Theory utilization rate %
(Mg _{70.6} Ni _{29.4}) ₉₈ La ₂	1016	347.8	34.2
(Mg _{70.6} Ni _{29.4}) ₉₅ La ₅	907	461.9	50.9
(Mg _{70.6} Ni _{29.4}) ₉₂ La ₈	814	564.2	69.3
(Mg _{70.6} Ni _{29.4}) ₉₀ La ₁₀	759	480.3	63.3
(Mg _{70.6} Ni _{29.4}) ₈₅ La ₁₅	642	456.3	71.1

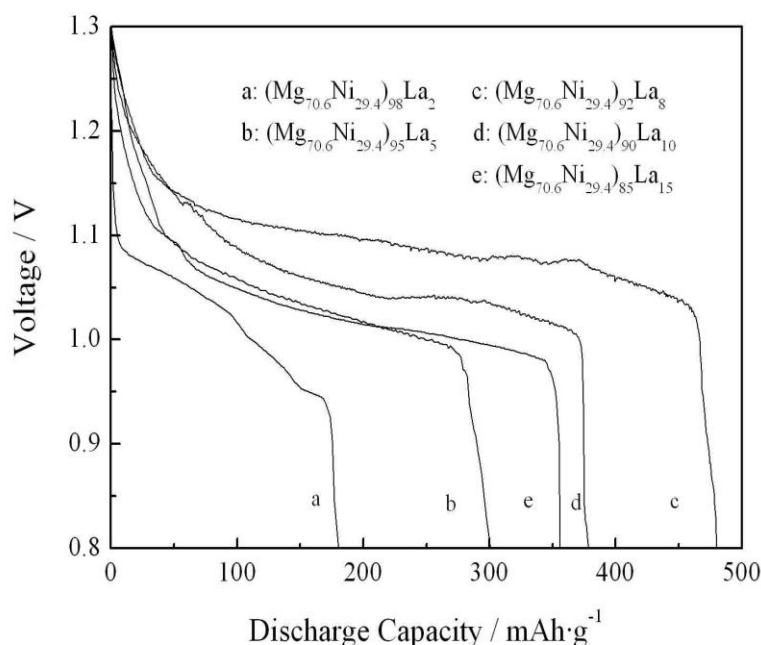


Figure 6. Relationship of voltage and the discharge capacities (at the 10th cycle) for Mg-Ni-La alloys.

According to the result of Orimo et al[25], hydrogen concentrations in three nanometer-scale regions and the maximum hydrogen concentrations of the three regions were experimentally determined to be 0.3 wt%H in the grain region, 4.0 wt%H in the grain boundary and 2.2 wt%H in the amorphous region. It reveals that the hydrides mainly exist in grain-boundary region and the amorphous phase region. Therefore, an optimum La content not only provides more amorphous phase and brings a refined microstructure for Mg-Ni-La alloys which enhanced absorption kinetics[26] but also effectively works as catalysts for the hydrogenations of Mg. Spassov et al.[27] observed an improvement in the hydrogenation kinetics of Mg₆₅Cu₂₅Y₁₀ alloy due to the catalytic effect of Yttrium.

The relationship of discharge potentials (voltage) and the discharge capacities (at the 10 cycles) is shown in Fig. 6. It is seen there that a discharge potentials flat from 1.2 to 1.0V for each alloy with variation of the discharge capacity which denotes a range of discharge capacity that the alloy can be used. It is found that the discharge capacities of the discharge potential flat have reached more than

400mAhg⁻¹ for alloys (Mg_{70.6}Ni_{29.4})₉₂La₈ and (Mg_{70.6}Ni_{29.4})₉₀La₁₀. However, the discharge capacity of the discharge potential flat of (Mg_{70.6}Ni_{29.4})₉₈La₂ alloy is only 181 mAhg⁻¹. It is also important to point out that the discharge capacity is significantly dependent on the composition and microstructure of the electrode materials.

Xuezhang et al. [28] and Khorkounov et al. [29] reported that the amorphous 2Mg–Fe + 150 wt.%Ni and Mg₆₁Ni₃₀Y₉ ribbons were synthesized by mechanical alloying. Wang et al. [30], Xu et al. [31] and Jurczyk et al. [32] also reported respectively that the amorphous Mg_{1.8}Nd_{0.2}Ni (the discharge capacity is 323.5 mAhg⁻¹), PrMgNi₄ (the discharge capacity is 254 mAhg⁻¹) and Mg_{1.5}Mn_{0.5}Ni ribbons (the discharge capacity is 241 mAhg⁻¹) were synthesized by mechanical alloying. From the above results, it is evident that the melt–spun ribbon (Mg_{70.6}Ni_{29.4})₉₂La₈ (the maximum discharge capacity is 564.2 mAhg⁻¹) showed superior hydrogenation kinetics and higher discharge capacity. One explanation for this could be the homogeneous microstructure of the melt–spun alloy. The as-cast eutectic alloy charged/discharged for some cycles consisted of lamellae of primary and secondary phases, where long continuous boundaries between primary and secondary phases could act as diffusion paths prior to hydrogen diffusion into the bulk. Zhu et al. [33] also reported that an auto-catalytic effect might govern the hydriding mechanism of the nanophase composite, while the hydriding process of single component alloys proceeds by means of a nucleation and growth mechanism.

4. CONCLUSIONS

The electrode properties of the rapidly solidified Mg–Ni–La amorphous alloys were examined. The results obtained are summarized as follows:

- 1). The single amorphous phase was obtained in the melt-spun (Mg_{70.6}Ni_{29.4})₉₂La₈, (Mg_{70.6}Ni_{29.4})₉₀La₁₀ and (Mg_{70.6}Ni_{29.4})₈₅La₁₅ ribbons.
- 2). In the cyclic life measurements, the discharge capacities increased with increasing La atomic content and the optimum La content is between 8 and 10 mol%. The highest discharge capacity reached more than 564.2 mAh g⁻¹ at the discharge current densities of 50mA g⁻¹ for (Mg_{70.6}Ni_{29.4})₉₂La₈ samples and the discharge capacity reaches 80% of the maximum discharge capacity after 10 cycles.
- 3). There is a discharge potential flat from 1.2 to 1.0V for each alloy with variation of the discharge capacity. The discharge capacities of the discharge potential flat have reached more than 400 mAh g⁻¹ for alloys (Mg_{70.6}Ni_{29.4})₉₂La₈ and (Mg_{70.6}Ni_{29.4})₉₀La₁₀.
- 4). It indicated that the amorphous structure was a key factor to achieve high discharge capacity and good cycling stability.

ACKNOWLEDGEMENTS

This work was supported by the China Postdoctoral Science Foundation (Grant No. 20100481299), Ph.D. Fund of Shandong Province(Grant No. BS2009C1039), Shandong Postdoctoral Innovation Fund (Grant No. 201003050) and Colleges and universities in Shandong Province science and technology projects Fund(Grant No. J11LD03).

References

1. D. Lupu, A. Biris, E. Indrea, *Int. J. Hydrogen Energy* 7 (1982) 783.
2. L. Schlabach, A. Zuttel, *Nature* 414 (2001) 353.
3. N. Cui, B. Luan, H.K. Liu, S.X. Dou, *J. Power Sources* 63 (1996) 209–214.
4. W. Liu, Y. Lei, D. Sun, J. Wu, Q. Wang, *J. Power Sources* 58 (1996) 243–247.
5. A. Gebert, B. Khorkounov, U. Wolff, C. Mickel, M. Uhlemann, L. Schultz, *J. Alloys Compd.* 419 (2006) 319–327.
6. K. Tanaka, *J. Alloys Compd.* 450 (2008) 432–439.
7. Q.F. Tian, Y. Zhang, L.X. Sun, F. Xu, Z.C. Tan, H.T. Yuan, T. Zhang, *J. Power Sources* 158 (2006) 1463–1471.
8. M. Zhu, H. Wang, L.Z. Ouyang, M.Q. Zeng, *Int. J. Hydrogen Energy* 31 (2006) 251–257.
9. J. Yin, K. Tanaka, N. Tanaka, *Mater. Trans.* 43 (3) (2002) 417.
10. G.I. Duarte, L.A.C. Bustamante, P.E.V. de Miranda, *Scripta Mater.* 56 (2007) 789.
11. S. Mokbli, M. Abdellaoui, H. Zarrouk, M. Latroche, A. PercheronGuégan, *J. Alloys Compd.* 460 (2008) 432–439.
12. D. Guzman, S. Ordonez, D. Serafini, P. Rojas, O. Bustos, *J. Alloys Compd.* 459 (2008) 425–432.
13. S.F. Santos, J.F.R. de Castro, T.T. Ishikawa, *J. Alloys Compd.* 434–435 (2007) 756.
14. St. Todorova, T. Spassov, *J. Alloys Compd.* 469 (2009) 193–196.
15. Lin-jun Huang, Jian-guo Tang, G.Y. Liang, Yao Wang, D.C. Wu, *J. Power Sources* 189 (2009) 1247–1250.
16. Lin-jun Huang, Jian-guo Tang, Yao Wang, Ji-xian Liu, D.C. Wu, *J. Alloys Compd.* 485 (2009) 186–191.
17. S. Loken, J.K. Solberg, J.P. Maehlen, R.V. Denys, M.V. Lototsky, B.P. Tarasov, V.A. Yartys, *J. Alloys Compd.* 446–447 (2007) 114–120.
18. K. Tanaka, Y. Kanda, M. Furuhashi, K. Saito, K. Kuroda, H. Saka, *J. Alloys Compd.* 293 (1999) 521–525.
19. H. Niu, D.O. Northwood, *Int. J. Hydrogen Energy* 27 (2002) 69–77.
20. X.Z. Xiao, X.H. Wang, L.H. Gao, L. Wang, C.P. Chen, *J. Alloys Compd.* 413 (2006) 312–318.
21. L.J. Huang, G.Y. Liang, Z.B. Sun, *J. Alloys Compd.* 421 (2006) 279.
22. L.J. Huang, G.Y. Liang, Z.B. Sun, Y.F. Zhou, D.C. Wu, *Mater. Sci. Eng. B* 141 (2007) 121.
23. L.J. Huang, G.Y. Liang, Z. B. Sun, Y.F. Zhou, *J. Alloys Compd.* 432 (2007) 172.
24. T. Spassov, U. Koster, *J. Alloys Compd.* 287 (1999) 243.
25. Orimoi S, Fujii H. *Appl Phys A*[J], 2001,72: 167
26. Savyak M, Hirnyj S, Bauer H D *et al. Journal of Alloys and Compounds*[J], 2004, 364: 229
27. Tony Spassov, Vellelina Rangelova, Nikolay Neykov. *Journal of Alloys and Compounds*[J], 2002, 334: 219
28. Xuezhang xiao, Xinhua Wang, Linhui Gao, Li Wang, Changpin Chen, *J. Alloys Compd.* 413 (2006) 312.
29. B. Khorkounov, A. Gebert, Ch. Mickel, L. Schultz, *J. Alloys Compd.* 458 (2008) 479.
30. Z.M. Wang, H.Y. Zhou, Z.F. Gu, G. Cheng, A.B. Yu, *J. Alloys Compd.* 381 (2004) 234–239.
31. X. Xu, H.Y. Zhou, R.P. Zou, S.L. Zhang, Z.M. Wang, *J. Alloys Compd.* 396 (2005) 247–250.
32. M. Jurczyk, L. Smardz, I. Okonska, E. Jankowska, M. Nowak, K. Smardz, *Int. J. Hydrogen Energy* 33 (2008) 374–380.
33. M. Zhu, Y. Gao, Z.X. Che, Y.Q. Yang, C.Y. Chuang, *J. Alloys Compd.* 330–332 (2002) 708.